EPJ Web of Conferences **364**, 15015 (2026) https://doi.org/10.1051/epjconf/202636415015
Quark Matter 2025

Search for the critical endpoint in high-statistics lattice QCD simulations

Alexander Adam[1,*] *Szabolcs* Borsányi[1], *Zoltán* Fodor[1,2,3,4], *Jana N.* Guenther[1], *Piyush* Kumar[1], *Paolo* Parotto[5], *Attila* Pásztor[4], and *Chik Him* Wong[1]

[1]Department of Physics, Wuppertal University, Gaussstr. 20, D-42119, Wuppertal, Germany
[2]Department of Physics, Pennsylvania State University, State College, PA 16801, USA
[3]Institute for Theoretical Physics, ELTE Eötvös Loránd University, Pázmány P. sétány 1/A, H-1117 Budapest, Hungary
[4]Jülich Supercomputing Centre, Forschungszentrum Jülich, D-52425 Jülich, Germany
[5]Dipartimento di Fisica, Università di Torino and INFN Torino, Via P. Giuria 1, I-10125 Torino, Italy

Abstract. One method to estimate the position of the critical endpoint of QCD is to model the free energy as a rational function of the baryon chemical potential μ_B and determine the Lee-Yang edge singularities. Using high-statistics simulations on 4HEX improved staggered $16^3 \times 8$ lattices by the Wuppertal-Budapest Collaboration we estimate the location of the closest singularity in the QCD phase diagram. Using this lattice setup we are able to reach an unprecedentedly low temperature of $T = 100$ MeV in our simulation dataset. To understand the true predictive power of such an approach, we analyze the systematic uncertainties of such an approach in detail. We compare various ansätze, including formulations that preserve baryon charge quantization by forcing the appropriate periodicity in the imaginary chemical potential. The parameters can be constrained by the cumulants of the net baryon density calculated with lattice simulations at $\mu_B^2 \leq 0$. Thus, we also compare single point and multipoint Padé approximations.

1 Introduction

Mapping the QCD phase diagram in the (T, μ_B) plane remains a key objective of heavy-ion physics. At vanishing chemical potential, the transition from hadronic matter to quark–gluon plasma is a crossover [1]. However, at finite density, the structure of the phase diagram and the possible existence of a critical endpoint are still uncertain.

The analysis procedure employed in this work, described in detail in Ref. [2], is based on simulations with $16^3 \times 8$ lattices using 4HEX staggered fermions, following earlier studies [3] but with greatly increased statistics. At zero chemical potential, around 2 million configurations per temperature were collected and around 100,000 configurations per temperature and imaginary chemical potential. This dataset makes it possible to determine baryon-number fluctuations $\chi_n = (\partial^n(p/T^4))/(\partial(\mu_B/T)^n)\big|_{\mu_B=0}$ with unprecedented accuracy, including pressure derivatives up to the tenth order. Figure 1 shows the resulting χ_n as functions of temperature. The fixed physical volume allows us to control the sixth and eighth orders with high precision, and here we report the first lattice determination of the tenth-order coefficient.

*e-mail: alexander.adam@uni-wuppertal.de

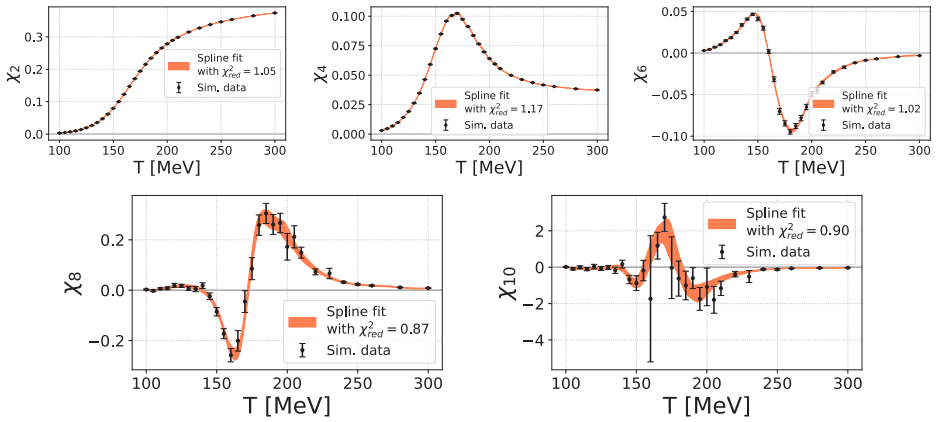

Figure 1. Temperature dependence of the pressure derivatives with respect to μ_B at $\mu_B = 0$ on $16^3 \times 8$ 4HEX ensembles. Curves indicate spline interpolations of the data points.

2 Results

The Lee-Yang zeros are the zeros of the partition function in the complex chemical potential plane. Their approach to the real axis reflects the nature of the transition. For a second-order phase transition, the scaling is given by [4] as $\mathrm{Im}\,\mu_B \sim V^{-\frac{\gamma/\nu+D}{2D}}$, which corresponds to $\mathrm{Im}\,\mu_B \sim V^{-0.83}$ for 3D Ising exponents. In the thermodynamic limit, the accumulation of zeros on the real axis generates the singularity of the free energy. When the volume correction is suppressed, the temperature dependence is dominated by $\mathrm{Im}\,\mu_B \sim |T - T_{\mathrm{CEP}}|^{\beta\delta}$.

To reach the complex plane, we use rational [m,n]-Padé $F[x]$ of the pressure, with the expansion variable $x = \cosh(\hat{\mu}_B) - 1 = \frac{1}{2}\hat{\mu}_B^2 + O(\hat{\mu}_B^4)$, $\hat{\mu}_B \equiv \mu_B/T$, which respects charge conjugation and Roberge-Weiss symmetries. For comparison, earlier works used $x = \mu_B$ [5] or $x = \mu_B^2$ [6]. This parameterization allows us to locate the leading Lee-Yang zeros and track their temperature dependence, providing estimates of the critical endpoint.

In Fig. 2 we show the fitted rational function in the interval $[0, i\pi]$ of imaginary μ_B/T, and its continuation to $[i\pi, i2\pi]$ using charge conjugation symmetry. This example, at $T = 135\,\mathrm{MeV}$, uses the $\Delta\hat{p}$ ansatz and χ_2 as the observable. The quantity $\Delta\hat{p}$ represents the pressure difference with respect to $T = 0$ and is obtained from the integral of χ_1. The fit includes $\chi_1, \ldots, \chi_4$ at eight imaginary valued chemical potentials, and $\chi_2, \ldots, \chi_{10}$ at $\mu_B = 0$. Both $\cosh(\hat{\mu}_B)$-Padé and μ_B^2-Padé describe the data well in $[0, i\pi]$, with the residuals shown in the lower panel. The benefit of $\cosh(\hat{\mu}_B)$-Padé becomes evident in the extended region, where it follows the mirrored data in contrast to μ_B^2-Padé.

The LYZ can be extracted from the denominator of the fitted ansatz by solving the roots algebraically. Each estimate of the leading Lee-Yang zero relies on an analytic continuation to complex chemical potentials, which can introduce systematic uncertainties. To assess these, we incorporate three different choices for F, namely $\Delta\hat{p}$, χ_1^B, and χ_2^B.

Assuming the CEP exists, universality arguments imply the asymptotic behavior of Eq. (2). Since our data are far from the CEP, an extrapolation over a large temperature range is required, which introduces additional systematic uncertainty. To assess this, we consider four different scaling ansätze with identical asymptotics but distinct behaviors away from criticality:

$$T - T_{CEP} \approx A_n \left(\mathrm{Im}\,\mu_{LY}^n\right)^{\frac{1}{\beta\delta}}, \quad n \in \{1, 2, 3, 4\}. \tag{1}$$

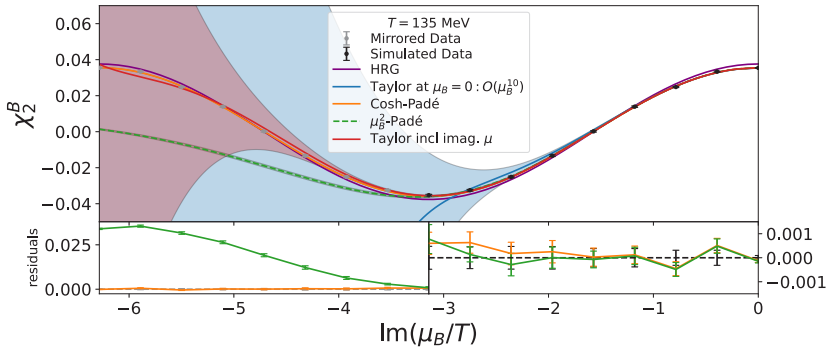

Figure 2. Fit of the Padé with $m = 1$ and $n = 2$, using $x = \cosh(\mu_B/T)$ (orange) and $x = \mu_B^2$ (green). Shown is the case $T = 135$ MeV with an ansatz for $\Delta\hat{p}$ in $[0, i\pi]$, extended to $[i\pi, i2\pi]$.

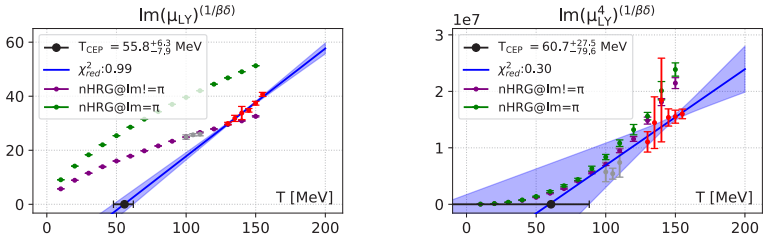

Figure 3. Extrapolation of the critical temperature using the two of the four different scaling ansätze. Near the CEP, all four ansätze are asymptotically equivalent, though farther away they lead to different behavior. The two (unstable) branches of the noisy HRG model (nHRG) baseline is also shown.

Figure 3 compares these fits with a non-critical baseline from an ideal hadron resonance gas including statistical noise (nHRG). Below $T = 130$ MeV the lattice results agree with the baseline and are therefore not constraining, so this range (shown in grey) is excluded from the fits. The resulting extrapolations yield CEP estimates spanning from the nuclear liquid–gas region to the high-temperature chiral regime.

An equally important source of uncertainty is the choice of the temperature range used in the fits. Lower temperatures are more reliable for extrapolating towards a Lee-Yang zero on the real μ_B axis, but they require higher statistics due to the unresolved sign problem. Within the available window $T = 130$–155 MeV, we therefore consider all six possible sub-windows that include at least four temperature points as part of the systematic analysis.

3 Conclusion

The three choices of F, the four scaling ansätze and six fitting windows result in 72 analyses. All fits have acceptable χ^2 values and are combined with uniform weights into a single cumulative distribution function (CDF) for T_{CEP}, assuming Gaussian distributions for the individual fits. The resulting distribution is shown in Fig. 4. With 84% probability the CEP lies below $T = 103$ MeV, or does not exist. If it exists, the most likely position (peak of the posterior distribution) is around $T = 70$ MeV.

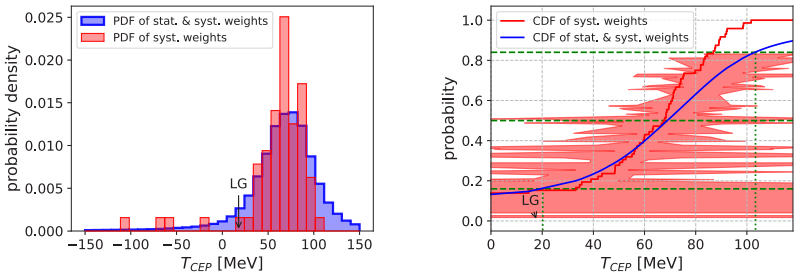

Figure 4. The histogram (left) and the cumulative distribution function for the critical endpoint temperature T_{CEP}. (We indicate the location of the liquid-gas critical endpoint with the label LG).

Acknowledgements

This work is supported by the MKW NRW under the funding code NW21-024-A. Further funding was received from the DFG under the Project No. 496127839. This work was also supported by the Hungarian National Research, Development and Innovation Office, NKFIH Grant No. KKP126769. This work was also supported by the NKFIH excellence grant TKP2021_NKTA_64. This work is also supported by the Hungarian National Research, Development and Innovation Office under Project No. FK 147164. This material is also based upon work supported by the National Science Foundation under grants No. PHY-2208724, and PHY-2116686, and within the framework of the MUSES collaboration, under grant number No. OAC- 2103680. This material is also based upon work supported by the U.S. Department of Energy, Office of Science, Office of Nuclear Physics, under Award Numbers DE-SC0022023 and DE-SC0025025, as well as by the National Aeronautics and Space Agency (NASA) under Award Number 80NSSC24K0767. The authors gratefully acknowledge the Gauss Centre for Supercomputing e.V. (www.gauss-centre.eu) for funding this project by providing computing time on the GCS Supercomputer HAWK at HLRS, Stuttgart. An award of computer time was provided by the INCITE program. This research used resources of the Argonne Leadership Computing Facility, which is a DOE Office of Science User Facility supported under Contract DE-AC02-06CH11357.

References

[1] Y. Aoki, G. Endrodi, Z. Fodor, S. Katz, K. Szabo, The Order of the quantum chromodynamics transition predicted by the standard model of particle physics, Nature **443**, 675 (2006), hep-lat/0611014. 10.1038/nature05120

[2] A. Adam, S. Borsányi, Z. Fodor, J.N. Guenther, P. Kumar, P. Parotto, A. Pásztor, C.H. Wong, High-precision baryon number cumulants from lattice QCD in a finite box: cumulant ratios, Lee-Yang zeros and critical endpoint predictions (2025), 2507.13254.

[3] S. Borsányi, Z. Fodor, J.N. Guenther, R. Kara, P. Parotto, A. Pásztor, L. Pirelli, C.H. Wong, Chiral versus deconfinement properties of the QCD crossover: Differences in the volume and chemical potential dependence from the lattice, Phys. Rev. D **111**, 014506 (2025). 10.1103/PhysRevD.111.014506

[4] C. Itzykson, R.B. Pearson, J.B. Zuber, Distribution of Zeros in Ising and Gauge Models, Nucl. Phys. B **220**, 415 (1983). 10.1016/0550-3213(83)90499-6

[5] D.A. Clarke, P. Dimopoulos, F. Di Renzo, J. Goswami, C. Schmidt, S. Singh, K. Zambello, Searching for the QCD critical endpoint using multi-point Padé approximations (2024), 2405.10196.

[6] D. Bollweg, J. Goswami, O. Kaczmarek, F. Karsch, S. Mukherjee, P. Petreczky, C. Schmidt, P. Scior (HotQCD), Taylor expansions and Padé approximants for cumulants of conserved charge fluctuations at nonvanishing chemical potentials, Phys. Rev. D **105**, 074511 (2022), 2202.09184. 10.1103/PhysRevD.105.074511